www.shd.org.rs

Journal of the Serbian Chemical Society

JSCS@tmf.bg.ac.yu • www.shd.org.rs/JSCS

J. Serb. Chem. Soc. *73* (6) 641–654 (2008) UDC 544.032.4:66.094.1:546.92+544.478+546.26
JSCS–3746 *Original scientific paper*

Temperature dependence of the kinetics of oxygen reduction on carbon-supported Pt nanoparticles

NEVENKA R. ELEZOVIĆ[1]*#, BILJANA M. BABIĆ[2], NEDELJKO V. KRSTAJIĆ[3], SNEŽANA LJ. GOJKOVIĆ[3] and LJILJANA M. VRAČAR[3]

[1]*Institute for Multidisciplinary Research, P. O. Box 33, Belgrade,* [2]*Vinča Institute of Nuclear Sciences, P. O. Box 522, 11001 Belgrade and* [3]*Faculty of Technology and Metallurgy, University of Belgrade, Karnegijeva 4, 11120 Belgrade, Serbia*

(Received 11 July, revised 20 November 2007)

Abstract: The temperature dependence of oxygen reduction reaction (ORR) was studied on highly dispersed Pt nanoparticles supported on a carbon cryogel. The specific surface area of the support was 517 m^2 g^{-1}, the Pt particles diameter was about 2.7 nm and the loading of the catalyst was 20 wt. %. The kinetics of the ORR at the Pt/C electrode was examined in 0.50 mol dm^{-3} $HClO_4$ solution in the temperature range from 274 to 318 K. At all temperatures, two distinct E–log j regions were observed; at low current densities with a slope of $-2.3RT/F$ and at high current densities with a slope of $-2.3\times2RT/F$. In order to confirm the mechanism of oxygen reduction previously suggested at a polycrystalline Pt and a Pt/Ebonex nanostructured electrode, the apparent enthalpies of activation at selected potentials *vs.* the reversible hydrogen electrode were calculated in both current density regions. Although $\Delta H^{\neq}_{a,l} > \Delta H^{\neq}_{a,h}$, it was found that the enthalpies of activation at the zero Galvani potential difference were the same and hence it could be concluded that the rate-determining step of the ORR was the same in both current density regions. The synthesized Pt/C catalyst showed a small enhancement in the catalytic activity for ORR in comparison to the polycrystalline Pt, but no change in the mechanism of the reaction.

Keywords: oxygen reduction reaction; platinum catalyst; carbon support; temperature dependence; enthalpy of activation.

INTRODUCTION

Platinum is the most active electrocatalyst for the oxygen reduction reaction (ORR) and it is still the only electrode material that can fulfill the demands for fuel cells working in acidic media. The kinetics of this reaction was extensively studied on smooth polycrystalline[1–8] and monocrystalline[6,9–14] Pt surfaces and on supported Pt nanoparticles,[15–22], as well as on Pt-based alloys[23–25] and Pt-al-

* Corresponding author. E-mail: nelezovic@tmf.bg.ac.yu
# Serbian Chemical Society member.
doi: 10.2298/JSC0806641E

loy nanoparticles.[19,26] Investigations on supported Pt nanoparticles are especially important because this type of electrocatalyst is employed for the fabrication of gas-diffusion electrodes in fuel cells with a solid polymer electrolyte (SPEFC). Most of the research was focused on the effects of loading,[17,21] particle size,[15–17] supporting material[17,22] and the influence of the alloying metal.[19,26] However, there has been little systematic research on the temperature dependence of the ORR on Pt nanoparticles, although SPEFCs operate at elevated temperatures. Paulus *et al.*[18] investigated the ORR on a Pt/Vulcan rotating disk electrode and found good agreement of both the Tafel slopes and the activation energy with the corresponding values on a single crystal[13] and polycrystalline Pt surfaces.[8] Yano *et. al.*[20] used a channel flow double electrode cell operating as a closed system in to order to eliminate any influence of temperature on the concentration of oxygen in the electrolyte. The activities of Pt/Carbon black and a bulk Pt film with and without a Nafion coating were investigated at temperatures in the range 30 to 110 °C. At all three electrodes, the current densities per real surface area and the apparent energy of activation agreed quite well, with the last being close to the results of Paulus *et al*.[18]

The temperature dependence of the ORR is not only important from the practical point of view, but it can also be used as a diagnostic tool for the elucidation of the mechanism of the reaction. A well established fact about the ORR on Pt is that the Tafel slopes differ at low and high current densities.[3,5,8–13,18–22] It was postulated that this is not caused by a change in the rate determining step but in the surface coverage by adsorbed intermediates. Šepa *et al.*[8] proved this by comparing the enthalpy of activation at zero Galvani potential difference for these two current density regions.

In this study, the temperature dependence of the ORR on Pt nanoparticles supported on a carbon cryogel was investigated in order to determine the mechanism of the reaction and to compare it with that of a polycrystalline Pt surface.

EXPERIMENTAL

Preparation of the catalyst

The catalyst used in the experiments was platinum nanoparticles supported on a carbon cryogel powder. The carbon cryogel was synthesized by a sol–gel polycondensation and freeze-drying; its BET surface area was 517 $m^2\ g^{-1}$.[27] The platinum was deposited on the support by a modified ethylene glycol method. The details of the preparation are given elsewhere.[28] The Pt loading of the catalyst was 20 wt. %.

Characterization of the catalyst

The Pt/C catalyst was characterized by X-ray diffraction (XRD) analysis and transmission electron microscopy (TEM). The XRD measurements were performed on a Siemens D500 X-ray diffractometer using CuKα radiation with a Ni filter. The 2θ angular region between 5 and 80° was explored at a scan rate of 0.02° s^{-1} with an angular resolution of 0.02° for all XRD tests.

The transmission electron microscopy (TEM) measurements were performed at the National Center for Electron Microscopy, USA, (NCEM) using an FEI (Phillips electronic instruments). The catalyst powder was suspended in ethanol, dropped onto a clean holey carbon grid and dried in air. The particle size distribution was determined from images of 20 different regions containing 10–20 particles each. The particle shape was determined by real space crystallography using high-resolution images taken from particles near or on the edge of the carbon black substrate and/or by numerical Fourier filtering of the digitized image intensity spectrum of particles on the top of the carbon.

Electrode preparation

The catalyst was applied to a gold substrate (6 mm diameter) in the form of a thin film. One milligram of Pt/C catalyst was mixed with 1.0 ml of water and 50 μl of Nafion solution (5 wt. %, Aldrich). The suspension was agitated in an ultrasonic bath for 60 min and 12.5 μl of it was placed on the gold electrode using a micro-pipette. After volatilization of the solvent, the electrode was heated at 80 °C for 10 min. The amount of Pt on the electrode was 2.5 μg, *i.e.*, 8.8 μg cm^{-2}.

Electrochemical measurements

A conventional three-compartment all-glass cell was used. The gold working electrode covered with a thin film of the Pt/C catalyst was in the form of rotating disk. The counter electrode was a platinum sheet of 5.0 cm^2 geometric area. A reversible hydrogen electrode in the same solution, maintained at room temperature in a compartment separated from the working electrode, was used as the reference electrode. All potentials are referred to the reversible hydrogen electrode (RHE). The electrolyte was 0.50 mol dm^{-3} $HClO_4$ solution (Spectrograde, Merck), prepared with high purity water (Millipore, 18 MΩ cm resistivity) at 293 K. The measurements were performed in the temperature range from 273 to 318 K.

Cyclic voltammetry was carried out in the electrolyte saturated with high purity nitrogen in the potential range from 0.03 to 1.40 V, at a sweep rate of 100 mV s^{-1}. Polarization curves of the ORR were recorded in the same solution saturated with O_2, bubbled continuously at 10^5 Pa pressure through the working electrode compartment. A slow linear sweep (1.0 mV s^{-1}) and a potentiostatic steady-state technique were applied. The electrode was rotated at 1600 rpm. An EG&G 273 potentiostat and a Philips PM 8143 X–Y recorder were employed in all the electrochemical experiments.

RESULTS AND DISCUSSION

Structure and particle size of the Pt/C catalyst

The XRD pattern of the Pt/C catalyst, given in Fig. 1, shows three characteristic reflection peaks: a peak at 2θ = 44.2°, corresponding to the hexagonal graphite structure (100) and peaks at about 39 and 46°, corresponding to the Pt (111) and Pt (200) plane, respectively. The first peak suggests good graphite characteristics of the carbon cryogel and the diffraction peaks of fcc Pt demonstrate a successful reduction of the Pt precursor to metallic Pt.

The low magnification TEM micrograph, presented in Fig. 2a, shows a very uniform Pt nanoparticles distribution. The mean particle size was determined as 2.7±0.7 nm. The atomically resolved image in Fig. 2b shows Pt atomic rows, with a spacing corresponding to the (200) and (111) planes of the fcc Pt nano-

particles, as indicated in the corresponding digital diffractogram also given in Fig. 2b. The Pt particles have the common cubo-octahedral shape. Occasionally twinned particles were observed with the same (111) twinning plane, as was observed with some other Pt-based catalysts.[29]

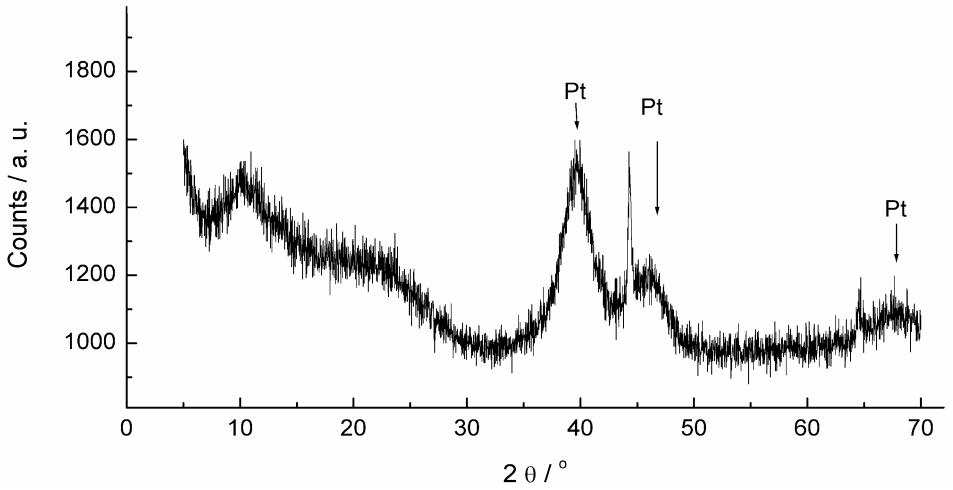

Fig. 1. X-Ray diffraction pattern of the Pt/C catalyst.

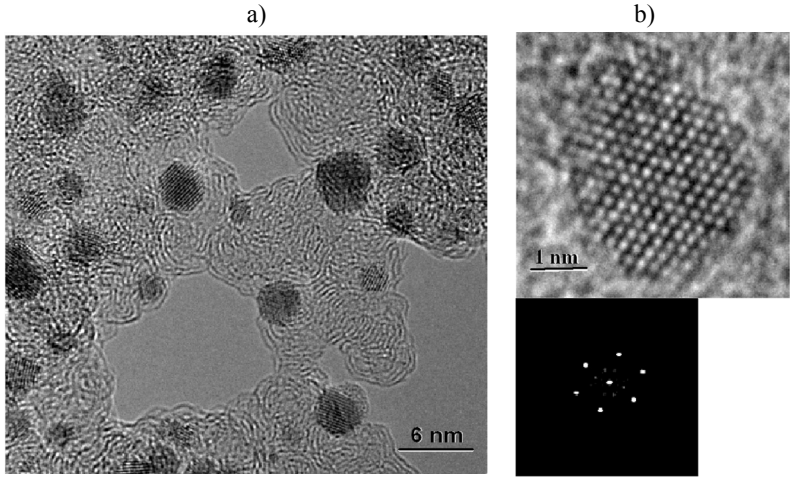

Fig. 2. TEM Images of the Pt nanoparticles on the carbon substrate; a) low magnification overview showing the spread of the Pt particles distribution on the carbon support; b) high resolution image showing the cubo-octahedral shape of a Pt particle.

Cyclic voltammetry of the Pt/C catalyst

The electrochemically active surface area is an implicit factor in the determination of the current density for any electrochemical reaction. This parameter

was determined from the steady-state cyclic voltammogram of Pt/C electrode in a 0.50 mol dm^{-3} $HClO_4$ electrolyte, shown in Fig. 3. The anodic part of the voltammogram, corresponding to hydrogen desorption, was integrated and the double-layer charging current subtracted. Assuming that 210 μC cm^{-2} corresponds to a monolayer coverage of adsorbed hydrogen, the surface area of the Pt nanoparticles was determined and the current densities for oxygen were calculated with respect to the surface area of that particular layer of the catalyst. The average value of the specific surface area of Pt particles was found to be 76 m^2 g^{-1}. Approximating the cubo-octahedral Pt particles as ideal spheres, a particle diameter of 3.7 nm was calculated. This value is larger that that obtained by TEM but this is to be expected because the surface of the supported catalyst particles in a thin film on the electrode is never completely accessible in the electrochemical experiments. However, taking into account also the fact that the carbon support material was also of high porosity, it is to be expected that some of the Pt particles were located in the inner part of the carbon support (micropores) and, consequently, were not electrochemically active (utility efficiency).

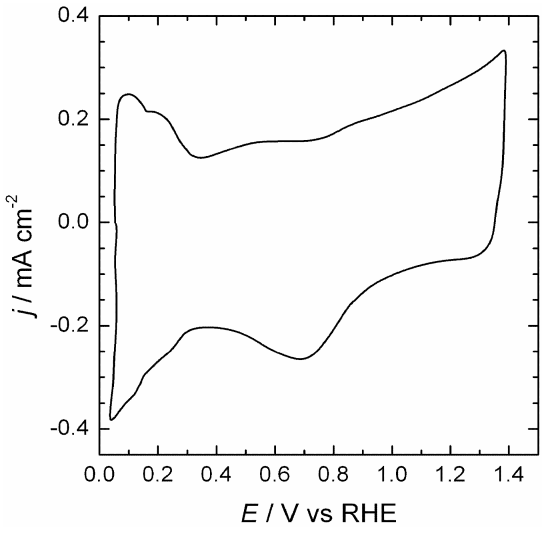

Fig. 3. Cyclic voltammetry curve for the Pt/C electrode at a sweep rate of 100 mV s^{-1} in a N_2-saturated 0.50 mol dm^{-3} $HClO_4$ solution at 298 K.

It should also be stressed that the current associated with the double layer is not constant with potential, meaning that the evaluation of the charge associated with UPD H would carry a certain error and this might explain the discrepancies between the average value of specific surface area found from integration of the UPD H peaks and average particle size from TEM images.

Kinetics of oxygen reduction

Since the ORR depends on the hydrodynamic conditions, a rotating Pt/C disk electrode was employed to measure the current densities of the reaction. The po-

larization curves for the ORR at different temperatures recorded with a slow potential sweep at an electrode rotating at 1600 rpm are shown in Fig. 4. The limiting current densities increased with temperature, indicating that the increase of the oxygen diffusion coefficient with temperature was higher than the decrease of oxygen solubility. A similar temperature dependence of the limiting current between 20 and 40 °C was reported in the literature.[18]

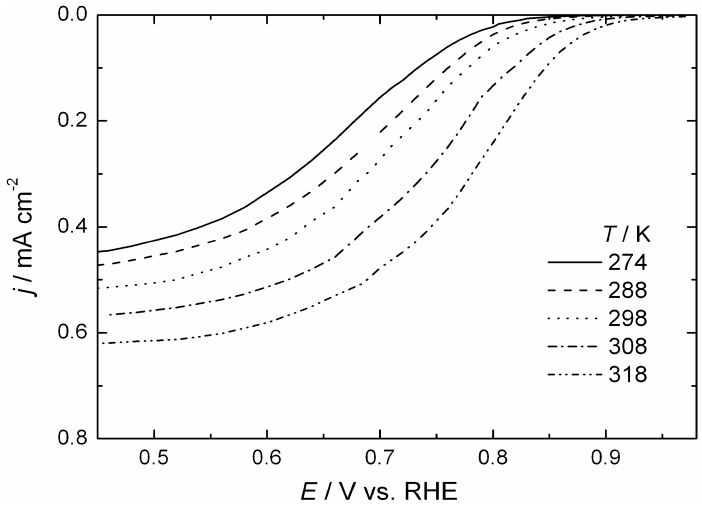

Fig. 4. Potentiodynamic (1.0 mV s^{-1}) polarization curves for the ORR at a Pt/C disk electrode rotating at 1600 rpm in a 0.50 mol dm^{-3} $HClO_4$ solution as a function of temperature.

For the kinetic analysis, the ORR current densities were determined by potentiostatic steady-state measurements because this technique corresponds better to real fuel cell conditions than linear sweep voltammetry. Also, a correction for the double layer charging current is avoided in steady-state measurements, which is important since the carbon cryogel support had a large surface area. After 30 min stabilization of the open circuit potential of the Pt/C electrode, potential steps of 30 s were applied in the ascending direction of overpotentials. These currents were corrected for the diffusion effects using the equation for the kinetic current density:

$$j_{\mathrm{kin}} = \frac{I_{\mathrm{L}} I}{I_{\mathrm{L}} - I} \times \frac{1}{S_{\mathrm{Pt}}} \tag{1}$$

where I is the measured current, I_{L} is the limiting current and S_{Pt} is the surface area of the Pt nanoparticles on the electrode, determined by cyclic voltammetry. The polarization curves, given as E *vs*. $\log j_{\mathrm{kin}}$ plots, at temperatures in the range from 273 to 318 K are shown in Fig. 5. In the whole examined temperature range, two distinct linear regions were observed, with Tafel slopes, b, increasing with temperature from 57 to 74 mV dec^{-1} at low current densities, and from 113 to 133 mV dec^{-1} at high current densities. In order to determine the transfer coeffi-

cients, the Tafel slopes were plotted as a function of temperature. Figure 6 shows the linear dependence on temperature in both current density regions. At high current densities, the *b vs*. *T* line follows the conventional dependence of–2.3*RT*/*βF,* with β being constant and close to 0.5. Such a conventional dependence, with β = = 1/2, is indicated in Fig. 6 by a broken line. At low current densities, the slope of *b vs*. *T* is close to –2.3*RT*/*F*. The Tafel slopes are similar to those on polycrystalline Pt.[3,5,9]

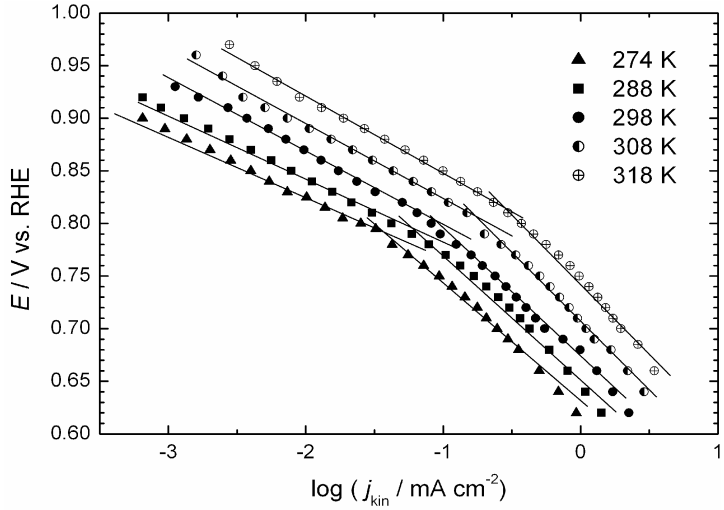

Fig. 5. Mass transfer corrected Tafel plots for the ORR on a Pt/C electrode in a 0.50 mol dm^{-3} $HClO_4$ solution for the temperature range 274–318 K.

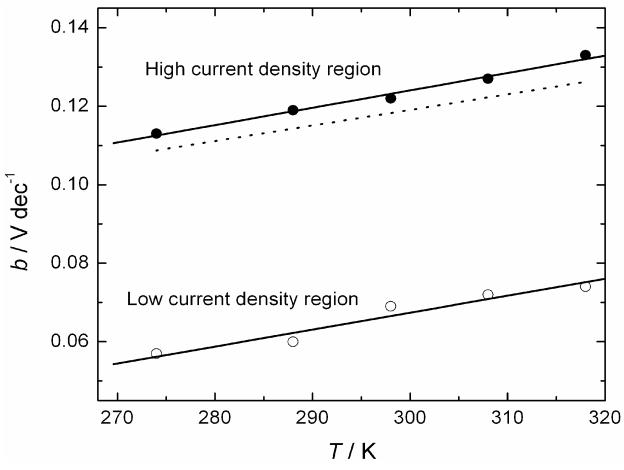

Fig. 6. Temperature dependence of the Tafel slope in low and high current density regions for the ORR at a Pt/C electrode in a 0.50 mol dm^{-3} $HClO_4$. The conventional dependence for β = 0.5 is indicated by the broken line.

The apparent enthalpy of activation of the oxygen reduction can be determined from the Arrhenius plot log j_{kin} *vs*. T^{-1}. However, since the concentration of dissolved oxygen in the electrolyte depends on the temperature, the kinetic

currents were normalized with respect to oxygen concentration at the given temperature.[30] The data for the potentials in low and high current density regions are presented in Fig. 7. The apparent enthalpies of activation were determined to be 69 kJ mol^{-1} at 0.900 V and 46 kJ mol^{-1} at 0.700 V. These values are higher than those reported in the literature,[18,20] which is probably the result of the different techniques employed for recording the polarization curves, *i.e.*, in this study, the steady-state technique was employed while in the others, the linear potential sweep technique was applied.

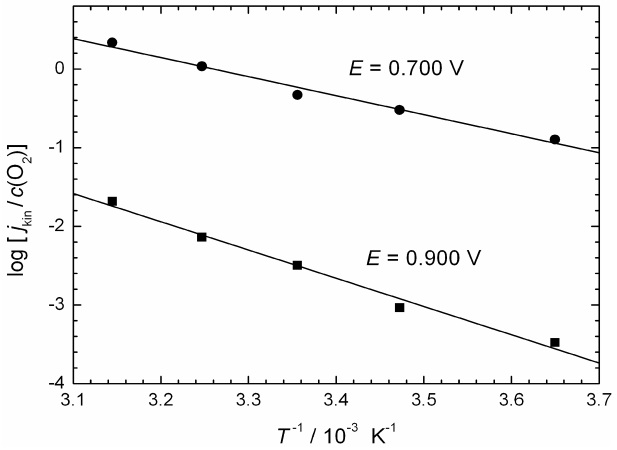

Fig. 7. Arrhenius plots for the ORR in a 0.50 mol dm^{-3} $HClO_4$ at a Pt/C electrode at potentials in the low and high current density regions. The mass transfer corrected currents were normalized with the respect to the concentration of dissolved oxygen.

The activity of the Pt/C catalyst for the ORR is compared with that of polycrystalline Pt in Fig. 8. For both electrodes, the current densities were calculated using the Pt surface area determined by cyclic voltammetry. As can be seen, the ORR current densities are higher on Pt/C catalyst than on polycrystalline Pt at more positive potentials while they are almost the same at potentials closer to the limiting current. The higher activity of Pt nanoparticles is probably the result of their surface structure. According to Sattler and Ross,[31] surface (111) and rough (110) regions dominate for particles of less than 3.5 nm. The TEM image of a Pt particle in the Pt/C catalyst used in this work (Fig. 2b) confirms that the (111) structure prevails in small particles. On the other hand, Marković *et al.*[12] showed that the activity for the ORR increased in the order (100) < (110) ≈ (111) in $HClO_4$ solutions.

Mechanism of the oxygen reduction reaction and apparent enthalpies of activation

A change in Tafel slopes with potential for an electrochemical reaction is usually explained by a change in the mechanism of the reaction. However, in the case of oxygen reduction, where adsorbed intermediates are involved, there is another possibility. For oxygen reduction on polycrystalline Pt, this was explained[5,8] by a change in the adsorption conditions of the adsorbed intermediates from

Temkin to Langmuirian. The same analysis as on polycrystalline Pt will be applied for oxygen reduction on the Pt/C nanostructured catalyst employed in this study.

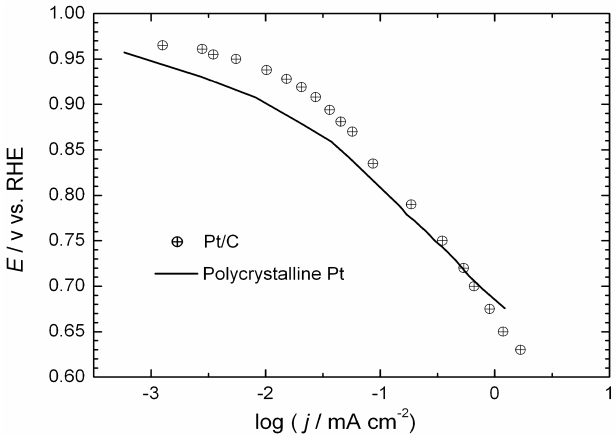

Fig. 8. Mass transfer corrected Tafel plots for the ORR at a Pt/C and a polycrystalline Pt electrode in a 0.50 mol dm^{-3} $HClO_4$ solution at 298 K.

According to Šepa *et al.*[5] the first step in oxygen reduction is the adsorption of molecular oxygen, which is followed by the slow transfer of an electron with or without the participation of an H_3O^+:

$$M + O_2 \rightleftarrows M\cdots O_2 \quad (2)$$

$$M\cdots O_2 + H_3O^+ + e^- \rightarrow \text{products} \quad (3)$$

or

$$M\cdots O_2 + e \rightarrow \text{products} \quad (4)$$

The rate equation for the proposed mechanism is:

$$j = k \exp(-\frac{\Delta G_0^*}{RT}) \exp[-\frac{\beta F(E - E_{\text{zop}})}{RT}] \quad (5)$$

where ΔG_0^* is the Gibbs energy of activation for the rate determining step at the zero Galvani potential difference, E_{zop} is the potential on the hydrogen electrode scale, at which the Galvani potential difference at the working electrode is zero[32] and k is the rate constant containing pH and oxygen partial pressure dependences of the individual rate equations as required for the steps (3) or (4).

Taking that the surface coverage by the adsorbed intermediates at high current densities is low, as was shown to be the case for both polycrystalline Pt[5] and Pt nanoparticles supported on Ebonex,[22] Langmuirian conditions prevail and ΔG_0^* is independent of the coverage, meaning that the reaction rate is:

$$j_{\text{h}} = k_{\text{h}} \exp(-\frac{\Delta G_{0,\text{h}}^*}{RT}) \exp[-\frac{\beta F(E_{\text{h}} - E_{\text{zop}})}{RT}] \quad (6)$$

where the subscript "h" denotes the high current density region.

In the low current density region, the coverage with the reaction intermediates is appreciable[5,22] and Temkin adsorption conditions must be considered. Since the adsorption energy of the reaction intermediate decreases with increasing coverage of oxygen species, the chemical part of the Gibbs energy of activation increases with the coverage:

$$\Delta G_\theta^* = \Delta G_0^* + \alpha r(\theta - \theta_\Gamma) \tag{7}$$

where θ_Γ is the transition level of surface coverage above which ΔG^* is affected by the coverage and where Langmuirian conditions change to Temkin conditions of adsorption, ΔG_0^* is the Gibbs energy of activation at low coverage ($\theta < \theta_\Gamma$), r is an energy parameter and α is a symmetry factor, usually taken to be 0.5. In the potential region where the Tafel slope is $-2.3RT/F$, the surface coverage θ was found to be linearly dependent on the electrode potential,[5] according to the relation:

$$\theta - \theta_\Gamma = \frac{F}{r}(E - E_\Gamma) \tag{8}$$

where E_Γ is the transition potential at which θ_Γ is reached, and the Tafel slope changed to $-2.3\times2RT/F$. Substituting Eq. (8) into Eq. (7), the Gibbs energy of activation is related to the electrode potential by:

$$\Delta G_\theta^* = \Delta G_0^* + \alpha F(E - E_\Gamma) \tag{9}$$

When Eq. (9) is introduced into the rate law (4), it takes the form:

$$j_l = k_l \exp(-\frac{\Delta G_{0,l}^*}{RT}) \exp[-\frac{F(\alpha E_l + \beta E_l - \alpha E_\Gamma - \beta E_{zop})}{RT}] \tag{10}$$

where the subscript "l" denotes the low current density region.

If rate determining step in the low and high current densities regions is the same, then the enthalpies of activation in these two regions will also be the same. Since the enthalpy of activation is a function of the electrode potential, the values at the same potential, *e.g.*, at the zero Galvani potential difference, are to be compared. In order to do this, Eqs. (9) and (10) have to be differentiated with respect to temperature. If it is assumed that the variation of the entropy of activation over the narrow temperature range of 40 °C is small and can be ignored, the enthalpies of activation at given potentials (E_h and E_l) *vs*. RHE, are given by the following equations:

$$\Delta H_{a,E_h}^* = -R(\frac{d\, ln\, j_h}{d(1/T)})_{E_h} = \Delta H_{0,h}^* + \beta F E_h - F E_{zop} + \frac{\beta F}{T} \times \frac{d(E_h - E_{zop})}{d(1/T)} \tag{12}$$

and

$$\Delta H^*_{\mathrm{a},E_\mathrm{l}} = -R\left(\frac{\mathrm{d}\,ln\,j_\mathrm{h}}{\mathrm{d}(1/T)}\right)_{E_\mathrm{l}} = \Delta H^*_{0,\mathrm{l}} + F(\beta E_\mathrm{l} + \alpha(E_\mathrm{l} - E_\mathrm{T})) - \beta F E_\mathrm{zop} + \\ + \frac{F}{T} \times \frac{\mathrm{d}(\alpha(E_\mathrm{l} - E_\mathrm{T}) + \beta(E_\mathrm{l} - E_\mathrm{zop}))}{\mathrm{d}(1/T)} \quad (13)$$

where $\Delta H^*_{0,\mathrm{h}}$ and $\Delta H^*_{0,\mathrm{l}}$ are the enthalpies of activation for the high and low current density regions at the zero Galvani potential difference. They cannot be experimentally determined because of the unknown E_zop, but their difference can be calculated using the apparent enthalpies of activation at the constant potential, $\Delta H^*_{\mathrm{a},E_\mathrm{h}}$ and $\Delta H^*_{\mathrm{a},E_\mathrm{l}}$:

$$\Delta^\mathrm{h}_\mathrm{l}(\Delta H^*_0) = \Delta H^*_{0,\mathrm{l}} - \Delta H^*_{0,\mathrm{h}} = \\ = \Delta H^*_{a,E_\mathrm{l}} - \Delta H^*_{a,E_\mathrm{h}} - F(\alpha E_\mathrm{l} + \beta E_\mathrm{l} - \beta E_\mathrm{h} - \beta E_\mathrm{T}) + \frac{\alpha F}{T} \times \frac{\mathrm{d}E_\mathrm{T}}{\mathrm{d}(1/T)} \quad (14)$$

It should be noted that the difference in the enthalpies at the zero Galvani potential depends neither on the position of the zero Galvani potential nor on the choice of the reference electrode.

Calculation of $\Delta^\mathrm{h}_\mathrm{l}(\Delta H^*_0)$ according to Eq. (14) requires the temperature dependence of the transition potential, E_T. The transition potentials were determined from the intersections of the Tafel lines in the low and high current density regions (Fig. 6) and plotted as a function of temperature in Fig. 9. All the data necessary for the calculation of $\Delta^\mathrm{h}_\mathrm{l}(\Delta H^*_0)$ at 298 K are given in Table I. As a result, $\Delta^\mathrm{h}_\mathrm{l}(\Delta H^*_0) \approx 1$ kJ mol^{-1} was obtained. Such a small difference can be ignored taking that $\Delta H^*_{0,\mathrm{l}} \approx \Delta H^*_{0,\mathrm{h}}$. This is the proof that oxygen reduction on the Pt/C catalyst followed the same mechanism in both the low and high current density regions. The difference in the Tafel slopes was not caused by different rate determining steps but by the change in the surface coverage and the adsorption conditions.

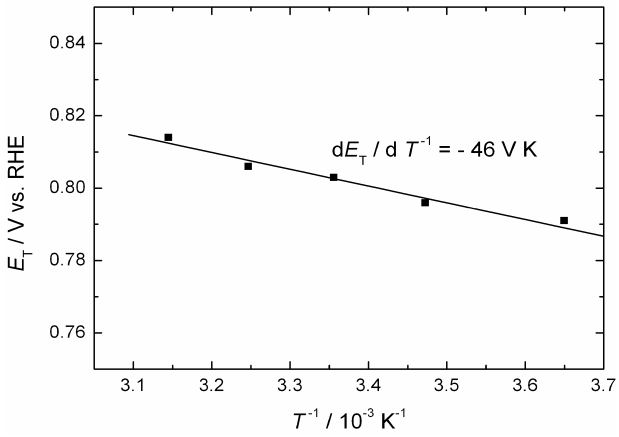

Fig. 9. Dependence of the transition potential on temperature for the ORR at a Pt/C electrode in a 0.50 mol dm^{-3} $HClO_4$ solution.

TABLE I. Data for the calculation of the difference in the enthalpies of activation at the zero Galvani potential for oxygen reduction on a Pt/C catalyst at 298 K: the apparent enthalpies of activation in the low and high current density region, the transition potential and its variation with temperature

$\Delta H^*_{\mathrm{a},E_\mathrm{l}=0.70\,\mathrm{V}}$ kJ mol^{-1}	$\Delta H^*_{\mathrm{a},E_\mathrm{h}=0.70\,\mathrm{V}}$ kJ mol^{-1}	$F\alpha E_\mathrm{T}$ kJ mol^{-1}	$\frac{\alpha F}{T}\times\frac{dE_\mathrm{T}}{d(1/T)}$ kJ mol^{-1}	$\Delta^\mathrm{h}_\mathrm{l}(\Delta H^*_0)$ kJ mol^{-1}
69±4	46±3	39	7.5	1

CONCLUSIONS

Platinum nanoparticles supported on a carbon cryogel showed activities for the ORR which was higher than that of polycrystalline Pt in the low current density region but the same in the high current density region. This is in accordance with literature data about preferential (111) and (110) faces on Pt nanoparticles smaller than 3.5 nm[31] and the higher activity of these planes for the ORR than the (100) plane.[12]

The Tafel slope values were $-2.3RT/F$ in the low current density region and $-2.3\times2RT/F$ in the high current density region, which is the same as on polycrystalline Pt. Therefore, an analysis of the apparent enthalpies of activation based on the proposed mechanism for oxygen reduction on polycrystalline Pt was performed. It was confirmed that the enthalpies of activation at the zero Galvani potential difference in both current density regions were the same, meaning that the same rate determining step of the ORR on Pt/C was operative in all potential regions, despite the changes in the Tafel slopes. The change in kinetics with potential arose from the different adsorption conditions of the reaction intermediates with potential. The values of the apparent enthalpies of activation, higher than those reported by applying linear potential sweep, could be the result of the steady-state technique used in the present experiments, which corresponds better to the real fuel cell conditions than linear sweep voltammetry.

Acknowledgement. This work was financially supported by the Ministry of Science of the Republic of Serbia, under Contact No. 142038.

И З В О Д

ТЕМПЕРАТУРНА ЗАВИСНОСТ ЕЛЕКТРОХЕМИЈСКЕ РЕДУКЦИЈЕ КИСЕОНИКА НА НАНОЧЕСТИЦАМА ПЛАТИНЕ НА УГЉЕНИЧНОМ НОСАЧУ

НЕВЕНКА. Р. ЕЛЕЗОВИЋ[1], БИЉАНА. М. БАБИЋ[2], НЕДЕЉКО. В. КРСТАЈИЋ[3], СНЕЖАНА. Љ. ГОЈКОВИЋ и ЉИЉАНА. М. ВРАЧАР[3]

[1]Институт за мултидисциплинарна истраживања, Београд, [2]Институт за нуклеарне науке "Винча", Београд и [3]Технолошко–металуршки факултет Универзитета у Београду, Београд

Кинетика реакције редукције кисеоника је испитивана на наночестицама платине дисперговaним на угљеничном носачу, у 0,50 mol dm^{-3} $HClO_4$, у температурном интервалу од 278 до 318 K. За синтезу Pt катализатора (Pt/C) је примењена модификована полиол метода

из раствора етилен гликола, док је као носач коришћен угљенични криогел. Катализатор је окарактерисан применом BET методе, дифракције X-зрака (XRD) и трансмисионе електронске микроскопије (TEM). Кинетика реакције редукције кисеоника испитивана је коришћењем стационарне поларизационе методе и методе цикличне волтаметрије. Област малих густина струје, на свим тепературама, на кривој поларизације, карактерише вредност Tafel-овог нагиба од $-2.3RT/F$, док је у области високих густина струје вредност овог нагиба $-2.3\times2RT/F$. Одређене су вредности привидне енталпије активације на константним потенцијалима, за обе области густина струја, и њихова разлика исказана за нулу Галванијеве разлике потенцијала. Потврђено је да је механизам редукције кисеоника, као и ступањ који одређује укупну брзину реакције исти у обе области густина струја, а да је разлика у кинетици реакције последица разлике у зависности адсорпције реакционих интермедијара од потенцијала. Поређењем каталитичке активности, изражене преко густине струје по реалној површини катализатора, констатована је нешто већа активност Pt/C катализатора у односу на поликристалну Pt.

(Примљено 11. јула, ревидирано 20. новембра 2007)

REFERENCES

1. A. Damjanović, M. A. Genshaw, J. O'M. Bockris, *J. Electrochem. Soc.* **114** (1967) 466
2. A. Damjanović, V. Brusić, *Electrochim. Acta* **12** (1967) 615
3. M. R. Tarasevich, *Elektrokhimiya* **9** (1973) 599 (in Russian)
4. M. R. Tarasevich, A. Sadkovski, E. Yeager in *Comprehensive Treatise of Electrochemistry, Vol. 7,* B. E. Conway, J. O'M. Bockris, S. V. M. Khan, R. E. White, Eds., Plenum Press, New York, 1983
5. D. B. Šepa, M. V. Vojnović, A. Damjanović, *Electrochim. Acta* **26** (1981) 781
6. R. Adžić, in *Electrocatalysis*, J. Lipkowski, P. N. Ross, Eds., Wiley, New York, 1998, p. 197
7. N. Wakabayashi, M. Takeichi, M. Itagaki, H. Uchida, M. Watanabe, *J. Electroanal. Chem.* **574** (2005) 339
8. D. B. Šepa, M. V. Vojnović, Lj. M Vračar, A. Damjanović, *Electrochim. Acta* **31** (1986) 1105
9. P. N. Ross, *J. Electrochem. Soc.* **126** (1979) 78
10. N. M. Marković, R. R. Adzić, B. D. Cahan, E. B. Yeager, *J. Electroanal. Chem.* **377** (1994) 249
11. N. M. Marković, H. A. Gasteiger, P. N. Ross, *J. Phys. Chem.* **99** (1995) 3411
12. N. Marković, H. Gasteiger, P. N. Ross, *J. Electrochem. Soc.* **144** (1997) 1591
13. B. N. Grgur, N. M. Marković, P. N. Ross, *Can. J. Chem.* **75** (1997) 1465
14. M. D. Maciá, J. M. Campiña, E. Herrero, J. M. Feliu, *J. Electroanal. Chem.* **564** (2004) 141
15. M. Watanabe, S. Saegusa, P. Stonehart, *Chem. Lett.* (1988) 1487
16. K. Kinoshita, *J. Electrochem. Soc.* **137** (1990) 845
17. S. Lj. Gojković, S. K. Zečević, R. F. Savinell, *J. Electrochem. Soc.* **145** (1998) 3713
18. U. A. Paulus, T. J. Schmidt, H. A. Gasteiger, R. J. Behm, *J. Electroanal. Chem.* **495** (2001) 134
19. U. A. Paulus, A. Wokaun, G. G. Scherer, T. J. Schmidt, V. Stamenković, N. M. Marković, P.N. Ross, *Electrochim. Acta* **47** (2002) 3787
20. H. Yano, E. Higuchi, H. Uchida, M. Watanabe, *J. Phys. Chem. B.* **110** (2006) 16544
21. E. Higuchi, H. Uchida, M. Watanabe, *J. Electroanal. Chem.* **583** (2005) 69
22. Lj. M. Vračar, N. V. Krstajić, V. R. Radmilović, M. M. Jakšić, *J. Electroanal. Chem.* **587** (2006) 99

23. V. Stamenković, T. J. Schmidt, P. N. Ross, N. M. Marković, *J. Phys. Chem. B.* **106** (2002) 11970
24. V. Stamenković, T. J. Schmidt, P. N. Ross, N. M. Marković, *J. Electroanal. Chem.* **554–555** (2003) 191
25. M. D. Obradović, B. N. Grgur, Lj. M. Vračar, *J. Electroanal. Chem.* **548** (2003) 69
26. U. A. Paulus, A. Wokaun, G. G. Scherer, T. J. Schmidt, V. Stamenković, N. M. Marković, P. N. Ross, *J. Phys. Chem. B.* **106** (2002) 4181
27. B. Babić, D. Đokić, N. Krstajić, *J. Serb. Chem. Soc.* **70** (2005) 21
28. B. M. Babić, Lj. M. Vračar, V. Radmilović, N. V. Krstajić, *Electrochim. Acta* **51** (2006) 3820
29. V. Radmilović, T. J. Richardson, S. J. Chen, P. N. Ross, *J. Catal.* **232** (2005) 99
30. D. Tromans, *Hydrometallurgy* **50** (1998) 279
31. M. L. Sattler, P. N. Ross, *Ultramicroscopy* **20** (1986) 21
32. A. J. Appleby, in *Modern Aspects of Electrochemistry*, *Vol. 9*, J. O′M. Bockris, B. E. Conway, Eds., Plenum Press, New York, 1974.